Building print-ready structures in biscale topology optimization framework

Dengyang Zhao[a] , Ming Li[a]*, Yusheng Liu[a] and Shuming Gao[a]

[a]State Key Laboratory of CAD&CG, Zhejiang University, Hangzhou, China
*E-mail: liming@cad.zju.edu.cn

Abstract

The self-supporting requirement is very necessary in additive manufacturing so that the printed structure will not collapse during fabrication. Imposing the self-supporting constraint on topology optimization allows for designing a performance optimized structure that is ready-to-print, and has recently attracted wide research interests. Different from these previous studies focusing on topology optimization in a single macro-scale, the paper proposes the first approach to constructing a self-supporting structure within a biscale topology optimization framework. It is first observed in this study that conducting self-supporting topology optimization iteratively for the macrostructure and separately for each microstructure is not sufficient to produce an overall self-supporting structure. As a particular contribution of the study, a novel approach to bridge the gap between the requirements of self-supporting at the two scales is proposed to resolve this issue via distinguishing macro-elements based on their relative locations. In addition, we express the self-supporting constraint as a simple quadratic function included in the topology optimization in both scales, and a carefully designed convolution operator is designed to efficiently implementing its detection. Ultimately, a completely self-supporting overall structure is generated within a biscale topology optimization framework, and extends the potentiality of topology optimization for structural design to be directly fabricated via additive manufacturing. Performance of the approach is also demonstrated via 2D and 3D examples.

Keywords –

Biscale topology optimization, self-supporting, print-ready, additive manufacturing.

1 Introduction

Topology optimization and additive manufacturing are natural counterparts to each other in that they have a very versatile capability of quickly generating and realizing new components that did not exist previously [1][2]. However, despite the enhanced geometric freedom associated with additive manufacturing, specific design rules must still be satisfied in order to ensure manufacturability. The fabrication overhang angle is an example of a rule of paramount importance to ensure that the part will not collapse when being fabricated layer by layer. A structure satisfying such an overhang angle constraint is called *self-supporting*. Thomas [3] identified 45 degrees as the typical maximum overhang angle through a large number of experiments, for example.

For a non self-supporting structure, its geometry has to be modified or additional *support* structures need to be generated. Modifying the geometry will ultimately reduce the structure's physical performance, while additional support raises the issues of automatic and minimum volume support design [4~9] and further post-processing activities to remove the unwanted supports. Due to these considerations, designing a self-supporting structure via topology optimization has thus become very important for practical applications and attracts the interest of various researchers. Brackett et al. [10] first suggested including the overhang angle constraint within a structure optimization framework. Various research efforts have since been conducted in very recent years, mainly based on filter-based SIMP approach [1,2,8,11,12,13], as will be detailed later on. These studies focus solely on the self-supporting topology optimization at the macro-scale.

In contrast, the paper studies the problem of designing a completely self-supporting structure within a biscale topology optimization framework. Inspired by biological systems, topology optimization can be conducted at both the macro-scale and micro-scale, called *biscale topology optimization*, to further improve their structural performance [14]. Within this biscale framework, each microstructure is associated to a macro-element, and its material property is estimated via a homogenization approach by performing FE analysis on the microstructure [15]. Extending the studies of self-supporting topology optimization in a single macro-scale to a concurrent biscale one will further broaden the potentiality of biscale topology optimization for

addictive manufacturing.

However, the extension is nontrivial. It is first observed in the study that simply imposing self-supporting constraint on each single microstructure or/and on the overall macrostructure will not produce a completely self-supporting structure due to the structural gap between the two scales. Specifically, the produced whole structure is not completely self-supporting in the microscale and may not be directly fabricated via additive manufacturing. The issue is resolved via a novel approach that performs microstructure topology optimization within different regions of design domains for differently located macro-elements. Ultimately, a completely self-supporting structure is generated in a biscale topology optimization framework. Its performance is also demonstrated via various 2D and 3D benchmark examples.

We also mention here that various excellent biscale topology optimization approaches have been proposed in the past, and considers different constraints on the microstructures. For example, Huang et al. [14] studied totally different microstructures to achieve best structural performance while Yan et al. [15] just considers microstructures of the same geometry for ease of convergence control, storage and fabrication. Furthermore, a constraint on material usage may be prescribed on the overall structure [15] or respectively on each single microstructure [14] for different design purposes. In order for the study to be more focused on the key issues on resolving self-supporting, we consider the case that the microstructures have the same geometry under a prescribed volume fraction. Its extensions to other cases of biscale topology optimization are to be explored in our future work.

In summary, the main contributions of the study are:

- The first approach to building self-supporting structure within a biscale topology framework, via a novel region-restricted topology optimization approach for microstructure design.
- A proper definition of the self-supporting constraints as a simple quadratic function included in the topology optimization in both scales, together with carefully designed convolution operators to efficiently implementing it.
- 2D and 3D benchmark examples to demonstrate performance of the approach.

The rest of the paper is organized as follows. Related work is first discussed in Section 2, and the biscale topology optimization problem under self-supporting constraints is formulated in Section 3. The numerical approach to tackle the problem is detailed in Section 4, followed by various 2D and 3D examples in Section 5. Finally, the paper is concluded in Section 6.

2 Related work

Since the first study in the late 1980s [16], various topology optimization approaches have been developed during the past decades, such as: homogenization [16], SIMP [17], BESO [18,19], level set [20,21], or more recently IGA [22] and others. See [23] for a recent and comprehensive review on this topic.

Most of the topology optimization techniques mainly focus on the one-scale design problem, either for the optimal design of macrostructures to improve their structural performance or for material design to develop new microstructures with prescribed or of extreme properties [16,24,25,26]. In particular, the latter assumes a periodic base cell distribution so that the macroscopic effective properties of the heterogeneous material can be averaged or homogenized according to the microstructure of the base cell. Such a microstructure design approach greatly enriches the availability of the material properties. However, material selection is actually a complex process involving not only the material properties but also the exterior boundary conditions. Thus recently, inspired by biological systems, people seek to concurrently design both the macrostructure and the material properties in terms of their microstructures [14,15]. Different from these studies, the proposed approach aims to take into account of the additional self-supporting constraint into the biscale optimization process for direct usage in additive manufacturing.

Actually, imposing various manufacturing constraint on topology optimization is a very important topic long studied. For example, Vatanabe et al [27] included various manufacturing constraints into topology optimization, such as minimum member size, minimum hole size, symmetry, pattern repetition, extrusion, turning, casting, forging and rolling. A recent excellent review on the topic is referred to [28]. Recent research efforts have also started to explore imposing self-supporting constraints into topology optimization due to the requirement from addictive manufacturing. Gaynor and Guest [11] generated the first self-supporting structure from topology optimization via a wedge-shaped filter in 2014. Later on, a novel and effective filter with smooth approximation to the minimum and maximum function was used by Langelaar to generate 2D [1] and 3D [2] self-supporting structures. Qian [12] presented an impressive approach to control both the undercut and the minimal overhang angle in a density-based topology optimization approach. Guo et al [13] included the self-supporting constraint as a set of explicit geometry parameters a topology optimization frameworks. A projection method in homogenization-based topology optimization was also recently prosed by Groen et al [29] to obtain manufacturable structures. In addition, Wu et al [8] solved the issue in a different viewpoint, via creating a

novel rhombic cell that can automatically satisfy the overhang constraint. Wang et al [30] overcame the difficulty of fabricating voids inside a solid via a support-free hollowing framework. Xie and Chen recently also generated support-free interior carving for 3D printing [31]. Impressive results were produced by the previous approaches. Different from these studies, imposing the self-supporting constraint within a biscale topology optimization framework is first studied here, built on our previous study on self-supporting topology optimization in macro-scale [32].

3 Problem statement and approach overview

In this section, the problem of biscale self-supporting topology optimization is mathematically formulated, and an overall approach to resolve it is explained. The self-supporting constraint is described here as a simple explicit quadratic function, and can be easily included in a topology optimization approach [32].

3.1 Definition of self-supporting constraint

The *supported elements* generally mean the structural elements that can be fabricated via additive manufacturing technologies without collapse during the fabrication process. They are defined here using a concept of a maximum printable supporting angle, or *overhang angle*, which is assumed to be 45 degrees, in accordance with a previous study [10]. Extensions of the approach to general overhang angles are also explained later. We assume in this section that the printing direction follows the positive-y axis direction, for ease of explanation.

Suppose we have a set of 2D discrete square element labeled as

$$\mathcal{M} = \{(\mathrm{n},\mathrm{m}) | 1 \le \mathrm{n} \le \mathrm{N}, 1 \le \mathrm{m} \le \mathrm{M}\}. \tag{1}$$

where n,m are the indices increasing along the x and y axes, respectively. We also use e to represent a square element without explicitly mentioning its indices n,m.

In addition, a density matrix $\boldsymbol{\rho}$ of size $\mathrm{N} \times \mathrm{M}$ is also associated to $\mathcal{M}$, where an entry value $\boldsymbol{\rho}(\mathrm{n},\mathrm{m}) = 1$ or 0, respectively, representing a solid or void element.

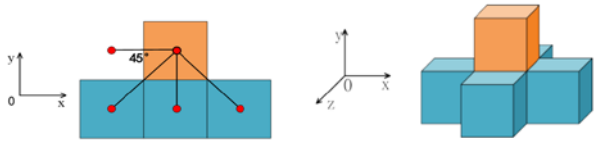

(a) 2D (b) 3D

Figure 1. An element (in orange) can be supported by one of the three supporting elements in blue.

As illustrated in Fig.1, given a density $\boldsymbol{\rho}$, a solid element $(\mathrm{n},\mathrm{m}) \in \mathcal{M}$ (in orange), it is *supported*, or called a *supported element*, if at least one of the three blue elements beneath it is solid. We formulate the self-supporting condition in a continuous form as follows: an element $(\mathrm{n},\mathrm{m}) \in \mathcal{M}$ is supported if its associated density matrix $\boldsymbol{\rho}$ satisfies

$$\sum_{\{\mathrm{n}-1<\mathrm{r}<\mathrm{n}+1\}} \boldsymbol{\rho}(\mathbf{r},\mathbf{m}-\mathbf{1}) > 0. \tag{2}$$

Correspondingly, the *supporting set* $\mathcal{M}_S(\boldsymbol{\rho})$ associated to $\boldsymbol{\rho}$ is the set of all its supported elements, that is,

$$\mathcal{M}_S(\boldsymbol{\rho}) = \{(\mathrm{n},\mathrm{m}) \in \mathcal{M} | \mathrm{m} = 1 \text{ or } \sum_{\{\mathrm{n}-1<\mathrm{r}<\mathrm{n}+1\}} \boldsymbol{\rho}(\mathbf{r},\mathbf{m}-\mathbf{1}) > 0\}. \tag{3}$$

Correspondingly, the set of unsupported elements to $\boldsymbol{\rho}$ is denoted

$$\mathcal{M}_U(\boldsymbol{\rho}) = \mathcal{M} \backslash \mathcal{M}_S(\boldsymbol{\rho}). \tag{4}$$

The self-supporting constraint, as first introduced in [32], is formulated below in terms of controlling the sum of squares of the unsupported elements' densities $\boldsymbol{\rho}$ under a very small positive value τ

$$U(\boldsymbol{\rho}) = \sum_{e \in \mathcal{M}_U(\boldsymbol{\rho})} \boldsymbol{\rho}_{\mathbf{e}}^{\ 2} \le \epsilon. \tag{5}$$

3.2 Biscale topology optimization under self-supporting constraint

Different from previous studies on topology optimization under self-supporting constraint at a single macro-scale, the self-supporting constraints on the microstructure are required. Direct optimization in the microscale is very computationally challenging, and we hope to resolve it in a biscale topology optimization framework. To properly state the problem, the self-supporting constraints are imposed both on the macro- and micro- structures, within the biscale topology optimization framework. Its further algorithmic improvement to produce an overall self-supporting structure in micro-scale will be further explained later.

In order that the paper is more focused on resolving the *biscale* self-supporting issue, it is assumed here that all the microstructures exhibit the same geometry all under the same prescribed volume constraint. Similar topic, without considering self-supporting constraint, was also studied in previous work [36].

Consider a design domain Ω under certain boundary conditions and external forces, as illustrated in Fig.2. Each macro-element is composed of a micro structure ω, which is assumed homogeneous throughout the macro-object Ω. The distribution of the macro-element is

described via a macro-density $\boldsymbol{\rho}$, and the distribution of micro-elements in ω is described via a micro-density $\mathbf{x}$. The optimization objective is to find the optimal topologies for both the macrostructure and the micro-structures, so that the resulted biscale structure has the minimal compliance under certain volume constraint. In addition, the self-supporting constraint is required at both the macro- and micro- scales.

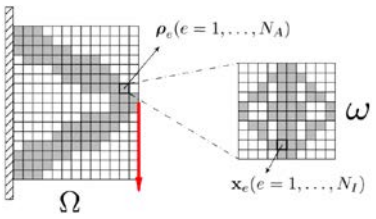

Figure 2. The problem of biscale topology optimization problem.

The problem is mathematically formulated as: find the optimal density distribution of $\boldsymbol{\rho}$, describing the macrostructure Ω, and distribution of $\mathbf{x}$, describing the microstructure ω, satisfying

$$\min_{\boldsymbol{\rho},\mathbf{x}} c(\boldsymbol{\rho},\mathbf{x}) = \mathbf{u}^{\mathrm{T}}\mathbf{K}(\boldsymbol{\rho},\mathbf{x})\mathbf{u}, st \tag{6}$$

$$\begin{cases} \mathbf{K}(\boldsymbol{\rho},\mathbf{x})\mathbf{u} = \mathbf{F}, \\ \sum_{1\le e\le \mathrm{N_A}} \boldsymbol{\rho}_e \le \mathrm{V_A}, \\ \sum_{1\le e\le \mathrm{N_I}} \mathbf{x}_e \le \mathrm{V_I}, \\ \boldsymbol{\rho}_{\min} \le \boldsymbol{\rho}_e \le 1, e = 1,\cdots,\mathrm{N_A}, \\ \mathbf{x}_{\min} \le \mathbf{x}_e \le 1, e = 1,\cdots,\mathrm{N_I}, \\ U(\boldsymbol{\rho}) = \sum_{e\in\mathcal{M}_U(\boldsymbol{\rho})} \boldsymbol{\rho}_e^{\,2} \le \epsilon_1, \\ U(\mathbf{x}) = \sum_{e\in\mathcal{M}_U(\mathbf{x})} \mathbf{x}_e^{\,2} \le \epsilon_2. \end{cases}$$

where $\mathbf{u}$ is the vector of global displacements, the objective function c is the compliance of the resulted biscale structure, $\mathbf{F}$ is the nodal force vector, $\mathrm{V_A}$, $\mathrm{V_I}$ are the prescribed volume usage, $\mathrm{N_A}$, $\mathrm{N_I}$ are element numbers at the macro-scale and micro-scale, respectively, and ϵ_1 and ϵ_2 are prescribed error bounds.

In addition, $\mathbf{K}(\boldsymbol{\rho},\mathbf{x})$ is the overall stiffness matrix at the macro-scale, defined as

$$\mathbf{K}(\boldsymbol{\rho},\mathbf{x}) = \sum_{e=1}^{\mathrm{N_A}} \boldsymbol{\rho}_e^{\mathrm{p}}\,\mathbf{K}_0(\mathbf{x}), \tag{7}$$

p (usually set as $\mathrm{p}=3$) is the penalty parameter, and $\mathbf{K_0}(\mathbf{x})$ is the elemental stiffness matrix defined as

$$\mathbf{K}_0(\mathbf{x}) = \int_\omega \mathbf{B}^{\mathrm{T}}\mathbf{D}^{\mathrm{MA}}(\mathbf{x})\mathbf{B}\mathrm{d}\omega, \tag{8}$$

where $\mathbf{B}$ is the strain-displacement matrix at the macro-scale, $\mathbf{D}^{\mathrm{MA}}(\mathbf{x})$ is the stiffness tensor of a solid element computed via homogenization for a microstructure ω,

$$\mathbf{D}^{\mathrm{MA}}(\mathbf{x}) = \frac{1}{|\omega|}\int_\omega \mathbf{x}^{\mathrm{p}}\mathbf{D}^{\mathrm{MI}}(\mathbf{I}-\mathbf{b}\boldsymbol{\mu})\mathrm{d}\omega = \mathbf{x}^{\mathrm{p}}\mathbf{D}^{\mathrm{MA}}, \tag{9}$$

where $\mathbf{D}^{\mathrm{MI}}$ is the micro element stiffness tensor, $\mathbf{b}$ is the micro strain-displacement matrix, and $\boldsymbol{\mu}$ is the vector of micro nodal displacement.

Note that the self-supporting constraint is essentially required for the overall microstructures, instead of respectively at the macro- and micro- scales. Actually, the requirements in Eq.(6) are not sufficient to produce an overall self-supporting structure in the micro-scale. The is because that the self-supporting constraint is imposed on each microstructure separately ignoring the inter-dependence between them. Additional strategy has to be further proposed to resolve the issue, as detailed next.

3.3 Overall approach

The biscale topology optimization problem is solved by iteratively computing the self-supporting structure at the macro-scale and micro-scale for minimal compliance of the overall structure. The optimization algorithm uses the classical MMA (Method of Moving Asymptotes) [37].

The overall procedure is depicted in Fig.3, and also explained below.

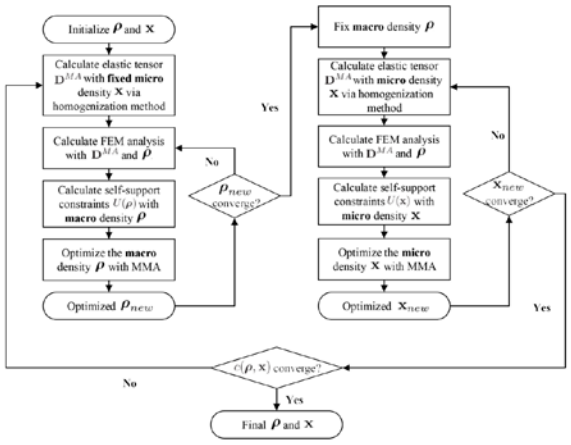

Figure 3. The flowchart of alternating iteration between two the macro- and micro- scales.

When computing in the macro-scale with a previously computed macro- density $\boldsymbol{\rho}$, the micro-structure density $\mathbf{x}$ is assumed fixed. The associated elasticity tensor $\mathbf{D}^{\mathrm{MA}}$ for $\mathbf{x}$ with respect to a macro- element can then be computed using homogenization approach, as described in Section 3.2. Then, the unsupported elements $\mathcal{M}_U(\boldsymbol{\rho})$ are detected via an efficient convolution operator, which

correspondingly gives the self-supporting constraint $U(\boldsymbol{\rho})$. After performing sensitivity analysis of the target and constraint with respect to the macro density $\boldsymbol{\rho}$, as further explained in Section 4.2, the MMA optimizer is applied to produce a self-supporting macro- structure until convergence.

Subsequently, when updating the micro-density $\mathbf{x}$, the the macro- density $\boldsymbol{\rho}$ is fixed. In order to bridge the self-supporting gap between the macro- and micro-scales, the macro-elements are classified into different types to produce self-supporting microstructures via topology optimization. Specifically, different design domains are selected for the these different types of macro-elements. After this, the overall optimization procedure just has one main difference from the macro-scale case - we need to compute the sensitivity of the optimization target and constraint with respect to the micro- density $\mathbf{x}$, instead of the macro- density $\boldsymbol{\rho}$. The chain rule will be involved in the step.

These two optimization procedures at the macro- and micro-scale are iterated until the optimization target $\boldsymbol{c}(\boldsymbol{\rho}, \mathbf{x})$ converges, ultimately producing the final optimized self-supporting structure.

4 Algorithmic aspects

4.1 Unsupported element detection

The problem in Eq.(6) requires detecting the un-self-supported elements $\mathrm{U}(\boldsymbol{\rho})$ or $\mathrm{U}(\mathbf{x})$. A direct enumeration would be very time-consuming, and a convolution operator is further introduced below to accelerate the detection process [32]. An acceleration of 10 times is observed experimentally owning to the usage of the convolution operator.

Its usage is based on the observation that an element is supported if the summation of the densities of its supporting elements is larger than zero. Thus, noticing that the overhang angle is 45 degrees, we introduce the following 2D self-supporting convolution kernel matrix $\mathbf{H}_0$,

$$\mathbf{H}_0 = \begin{pmatrix} 1 & 1 & 1 \\ 0 & 0 & 0 \\ 0 & 0 & 0 \end{pmatrix}. \tag{10}$$

Accordingly, a new matrix $\boldsymbol{\rho}$ indicating the supported elements can be computed via performing the convolution between the density matrix $\boldsymbol{\rho}$ and $\mathbf{H}$, that is,

$$\boldsymbol{\rho}_{\mathrm{S}} = \mathrm{sign}(\boldsymbol{\rho} * \mathbf{H}) \wedge \boldsymbol{\rho}, \tag{11}$$

where $\wedge$stands for element-wise boolean "and", $\boldsymbol{\rho} * \mathbf{H}$ is the convolution between matrices $\boldsymbol{\rho}$ and $\mathbf{H}$, and the sign function

$$\mathrm{sign(x)} = \begin{cases} 0, & \text{if } \mathrm{x} = 0 \\ 1, & \text{if } \mathrm{x} > 0' \end{cases} \tag{12}$$

Procedure of performing the convolution operator is also depicted in Fig.4.

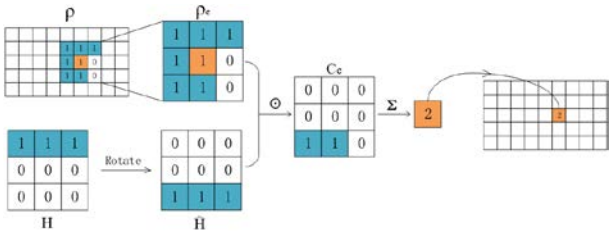

Figure 4. The discrete convolution procedure in 2D for detecting supported elements using the designed self-supporting Kernel matrix $\mathbf{H}$.

Correspondingly, the matrix $\mathbf{U}$ of unsupported elements can be computed efficiently as follows,

$$\mathbf{U} = \boldsymbol{\rho} - \mathrm{sign}(\boldsymbol{\rho} * \mathbf{H}) \wedge \boldsymbol{\rho}, \tag{13}$$

where $\boldsymbol{\rho}$ is taken as a 0-1 matrix.

4.2 Sensitivities analysis

First consider the macrostructure design, where the microstructure density $\boldsymbol{\rho}$ is taken as fixed. The overall structural compliance can be expanded as the sum of each element, that is,

$$\mathrm{c}(\boldsymbol{\rho}, \mathbf{x}) = \mathbf{u}^{\mathrm{T}}\mathbf{K}(\boldsymbol{\rho}, \mathbf{x})\mathbf{u} = \sum_{\mathrm{e}=1}^{\mathbf{N}_{\mathrm{A}}} \boldsymbol{\rho}_{\mathrm{e}}^{\mathrm{p}} \mathbf{u}_{\mathrm{e}}^{\mathrm{T}} \mathbf{K}_0(\mathbf{x}) \mathbf{u}_{\mathrm{e}}, \tag{14}$$

Accordingly, the sensitivity, or the partial derivative, of the compliance c with respect to the macro density $\boldsymbol{\rho}$ is given:

$$\frac{\partial \mathrm{c}}{\partial \boldsymbol{\rho}_e} = \mathrm{p}\boldsymbol{\rho}_{\mathrm{e}}^{\mathrm{p}-1} \mathbf{u}_{\mathrm{e}}^{\mathrm{T}} \mathbf{K}_0(\mathbf{x}) \mathbf{u}_{\mathrm{e}}, \tag{15}$$

where $\mathbf{K}_0$ is a constant matrix for a fixed $\mathbf{x}$, and $\mathbf{u}_{\mathrm{e}}$ is the displacement with respect to an element e.

Next consider the microstructure design, where the macrostructure $\boldsymbol{\rho}$ is taken as fixed. Accordingly, the partial derivative of the overall compliance with respect to each micro-element density $\mathbf{x}_{\mathrm{i}}$ is derived as follows,

$$\frac{\partial \mathrm{c}(\boldsymbol{\rho}, \mathbf{x})}{\partial \mathbf{x}_{\mathrm{i}}} = \sum_{\mathrm{e}=1}^{\mathbf{N}_{\mathrm{A}}} \boldsymbol{\rho}_{\mathrm{e}}^{\mathrm{p}} \mathbf{u}_{\mathrm{e}}^{\mathrm{T}} \left(\int_{\omega} \mathbf{B}^{\mathrm{T}} \frac{\partial \mathbf{D}^{\mathrm{MA}}(\mathbf{x})}{\partial \mathbf{x}_{\mathrm{i}}} \mathbf{B} \mathrm{d}\omega \right) \mathbf{u}_{\mathrm{e}}, \tag{16}$$

In particular, the partial derivative of the stiffness tensor computed by homogenization is derived as,

$$\frac{\partial \mathbf{D}^{\mathrm{MA}}(\mathbf{x})}{\partial \mathbf{x}_{\mathrm{i}}} = \frac{\mathrm{p}\mathbf{x}^{\mathrm{p}-1}}{|\omega|} \int_{\omega} \mathbf{D}^{\mathrm{MI}} (\mathbf{I} - \mathbf{b}\boldsymbol{\mu}_{\mathrm{i}}) \mathrm{d}\omega, \tag{17}$$

According to the chain rule, the partial derivative of compliance c with respect to the micro-density $\mathbf{x}$ can be derived by substituting (17) into (16).

The sensitivity of the self-supporting constraint is

straightforward, which ultimately results in a linear function in terms of the design density $\brho$ in the macro- case, that is,

$$\frac{\partial U(\boldsymbol{\rho})}{\partial \boldsymbol{\rho}_e} = \begin{cases} 2\boldsymbol{\rho}_e, & \text{if } e \in \mathcal{M}_U(\boldsymbol{\rho}) \\ 0, & \text{if } e \notin \mathcal{M}_U(\boldsymbol{\rho}) \end{cases}, \tag{18}$$

The case in the the micro- density **x** is similarly derived.

4.3 Types of micro-scale design domains in 2D

As explained previously, conducting the self-supporting topology optimization both for the macrostructure and for each microstructure cannot produce a totally overall self-supporting structure. We further classify the macro-elements in 2D into four types of design domains to resolve the issue. In addition, a novel efficient convolution operator is also introduced to classify these types for computational efficiency.

Consider the example in Fig.5. The derived overall structure in the macro-scale after classical topology optimization, without considering self-supporting constraint, is given in Fig.5(a). If performing one more cycle of self-supporting topology optimization at the micro-scale, the structure in Fig.5(b) is obtained. Some unsupported elements in micro-scale are observed in the resulted structure, which are respectively shown in red, yellow and orange in Fig.5(b) to indicate their different types of locations. Using the proposed approach, on the other hand, will produce a completely self-supporting structure shown in Fig.5(c). It consists of four types of different microstructures depending on the locations of their associated macro-scale design domains.

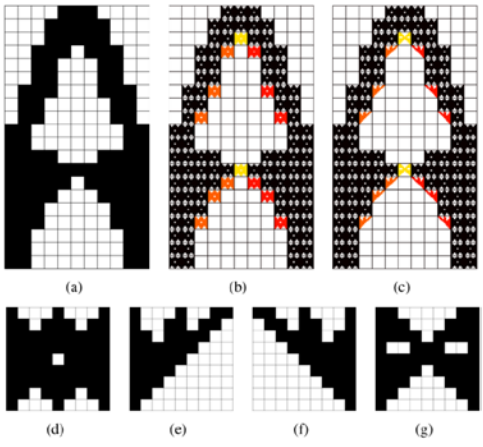

Figure 5. The self-supporting macro- and micro-structures: (a) is a self-supporting macro structure, (b) is a two-scale self-supporting structure not ready to be fabricated and the colored elements cannot be supported, (c) is a modified two-scale self-supporting structure which can be manufactured, (d) is a self-supporting microstructure embedded in the black elements in (c); (d),(e),(f) are self-support microstructures embedded in the orange, red and yellow elements in (c) respectively.

The proposed approach is based on the observation that a microstructure cannot be fully supported owing to the fact that its bottom elements are not supported. In order to resolve this issue, a proper design domain for the microstructure optimization within each macro-element has to be properly selected. The selection is based on relative locations of these macro-elements, and we classify them into four different types (see also Fig.6(a)): *edge-supported*(in blue), *left-corner supported*(in red), *right-corner supported*(in orange) and *two-corner supported* (in green). Different types determine different regions of design domains, as illustrated in orange in Fig.6(b-e).

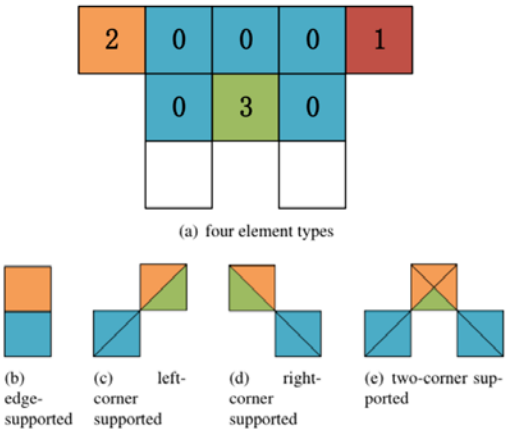

Figure 6. The macro-elements in 2D are classified into four types according to the range of their micro-elements to be supported: edge-supported (blue element 0), left-corner supported (red element 1), right-corner supported (orange element 2), two-corner supported (green element 3). The different types determine different design domains (in orange) for self-supporting microstructure design, as shown in (b-e).

Directly detecting the four different types of macro-elements via simple enumeration is very time consuming. We further accelerate the process via introducing novel convolution operations. Specifically, similar as the definition of the convolution kernel matrix $\mathbf{H}_0$ in Eq.(10), the following three convolution kernel matrices are introduced:

$$\mathbf{H}_1 = \begin{pmatrix} 0 & 0 & 1 \\ 0 & 0 & 0 \\ 0 & 0 & 0 \end{pmatrix}, \mathbf{H}_2 = \begin{pmatrix} 1 & 0 & 0 \\ 0 & 0 & 0 \\ 0 & 0 & 0 \end{pmatrix}, \mathbf{H}_3 = \begin{pmatrix} 1 & 0 & 1 \\ 0 & 0 & 0 \\ 0 & 0 & 0 \end{pmatrix} \tag{19}$$

Conducting a convolution operation between the density matrix $\boldsymbol{\rho}$ with each kernel gives

$$\boldsymbol{\rho}_i = \boldsymbol{\rho}_i * \mathbf{H}_i, (i = 0,1,2,3), \tag{20}$$

whose entry value indicates the number of elements supporting the element in this location.

We also define an indication matrix $\delta(\tilde{\boldsymbol{\rho}}, q)$ to represent whether an entry value of a matrix $\tilde{\boldsymbol{\rho}}$ is equal to a specified value, specifically,

$$\delta_{nm}(\tilde{\boldsymbol{\rho}}, q) = \begin{cases} 1, & \text{if } \tilde{\boldsymbol{\rho}}(n,m) = q \\ 0, & \text{if } \tilde{\boldsymbol{\rho}}(n,m) \neq q' \end{cases} \tag{21}$$

for an integer $0 < q < 3$.

Using the indication matrix $\delta(\tilde{\boldsymbol{\rho}}, q)$, the four types of macro-elements can be accordingly determined via the following four different types of matrices:

$$\begin{cases} \mathbf{W}_1 = \delta(\boldsymbol{\rho}_0, 1) \wedge \delta(\boldsymbol{\rho}_1, 1) \wedge \boldsymbol{\rho}, \\ \mathbf{W}_2 = \delta(\boldsymbol{\rho}_0, 1) \wedge \delta(\boldsymbol{\rho}_2, 1) \wedge \boldsymbol{\rho}, \\ \mathbf{W}_3 = \delta(\boldsymbol{\rho}_0, 2) \wedge \delta(\boldsymbol{\rho}_3, 2) \wedge \boldsymbol{\rho}, \\ \mathbf{W}_4 = \text{sign}(\boldsymbol{\rho}_0) - \mathbf{W}_1 - \mathbf{W}_2 - \mathbf{W}_3, \end{cases} \tag{22}$$

where $\mathbf{W}_1 = 1$ indicates the set of right-corner supported elements, $\mathbf{W}_2 = 1$ left-corner supported elements, $\mathbf{W}_3 = 1$ two-corner supported elements and $\mathbf{W}_0 = 1$ edge-supported elements.

After identifying these different types of macro-elements, the self-supporting microstructure optimization is performed in each type of corresponding design domain, that is, the orange region in Fig.6. In addition, in order to control the connectivity between adjacent micro structures, the symmetry requirement is also imposed on $\mathbf{W}_1$.

4.4 Types of micro-scale design domains in 3D

Extension of the above approach to 3D case follows a similar procedure, but has to consider much more types of macro-element locations, as explained below.

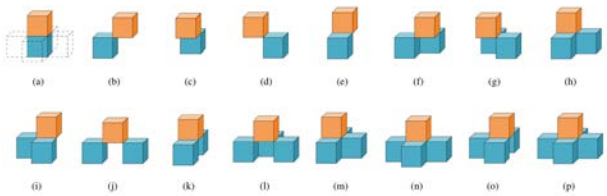

Figure 7. The macro-elements in 3D are classified into sixteen types according to the range that their micro-elements are to be supported, and have three different situations. The first is the one supported right by the element beneath it (in (a)), the second is the four basic types shown in (b-e). The other types can be seen as combinations of these situations shown in (f-p).

In 3D situation, an element is supported if at least one of the five elements beneath it exists, as can be seen in Fig. 1(b). Accordingly, the 3D macro-elements can be classified into sixteen types according to their relative locations, as depicted in Fig.7. They have three different situations. The first is the one supported right by the element beneath it (in (a)), the second is the four basic types shown in (b-e). The other types can be seen as combinations of these situations, as shown in (f-p). Correspondingly, similar as 2D case, the design domain for the self-supporting microstructure optimization can be obtained. Fig.8 gives the corresponding design domains for the four basic types in Fig.7(b-e). Other cases are obtained as the combination of the four basic design domains according to the type of the macro-elements, and are not further explained here.

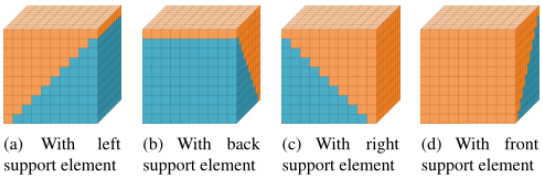

Figure 8. The four basic design domains for designing self-supporting microstructure.

4.5 Extensions to general overhang angles

This above described approach can also be extended to deal with cases of general overhang angles larger or smaller than 45 degrees. As can be seen in Fig.9(a), if the angle is smaller than 45 degrees, only the orange elements are chosen as the domain for its associated microstructure design. However, the case that the overhang angle is larger than 45 degrees cannot be similarly handled as this, as it otherwise would produce disconnected micro-structures, as illustrated in Fig.9(b). In this case, all the FE elements are not generated as square or cubic elements, and are instead scaled to rectangular domains as shown in Fig.9 (c).

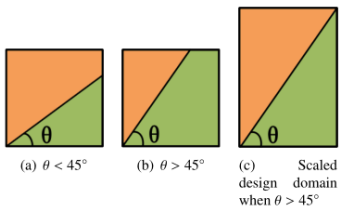

Figure 9. The design domain in a macro-element used for self-supporting microstructure generation with overhang angle θ different from 45 degrees.

5 Numerical performances

Various numerical examples are presented to test performance of the proposed approach. For illustration purposes, the load and geometry data are chosen to be dimensionless. The Young's modulus and Poisson's ratio of the solid material are set as $E = 1$ and $\upsilon = 0.3$ for all examples. The overhang angle is set to 45 degrees and the printing direction is selected during each optimization

process and marked in each example figure.

5.1 2D cantilever

Fig.10 shows the classic cantilever problem in a rectangular domain of size 60×20 with a concentrated vertical loading at the center of the right edge. In addition, each macro-element consists of 15×15 square micro-elements. The total number of micro-elements becomes 900×300 in this case. The target volume fraction is 50% at the macro-scale and 60% at the micro-scale. The maximal iteration step is set to 200 at each scale. The printing direction is chosen from left to right.

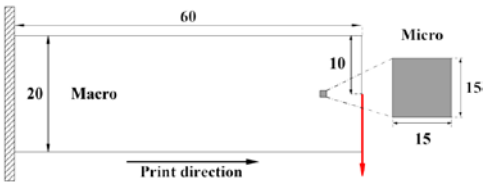

Figure 10. The design domain of a two-scale cantilever problem.

5.1.1 Optimized structure

The final optimized structure is shown in Fig.11, where the macrostructure and the associated microstructures, associated to the four different types of macro-elements in different colors, are respectively shown in (a) and (c-f). Ultimately, the produced print-ready structure is plotted in Fig.11(b) with its close-up. As can be seen from the results, by further classifying the four different types of macro-elements in the micro-scale optimization process, a completely self-supporting structure is produced.

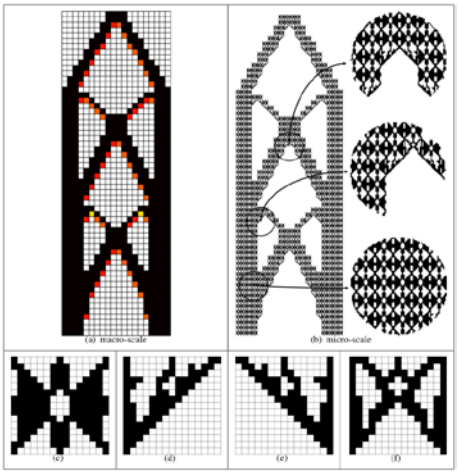

Figure 11. The produced self-supporting biscale structure for the cantilever example in Fig.10, where the four micro-structures for the four types of macro-elements in Fig.5 are plotted in the bottom.

The optimization target, or the compliance, of our derived structure is 175.4. We also compare it with two other benchmark results. Firstly, we conducted a single-scale optimization at macro-scale at size 60×20 with a volume fraction 0.3, which gives a structure of compliance 157.6. Secondly, we conducted a single-scale optimization at micro-scale at size 900×300 with volume fraction 0.3, which gives another structure of compliance 137.3. As can be seen from the comparison, compliance of the derived structure is larger than those of the other two. This is reasonable considering the additional constraints on self-supporting and on each micro-structure; see also Eq.(6).

5.1.2 Procedure

The structure is derived by iteratively performing topology optimization at the macro-scale and at the micro-scale. The entire optimization process takes 1026 steps to obtain the final multi-scale design shown in Fig.11.

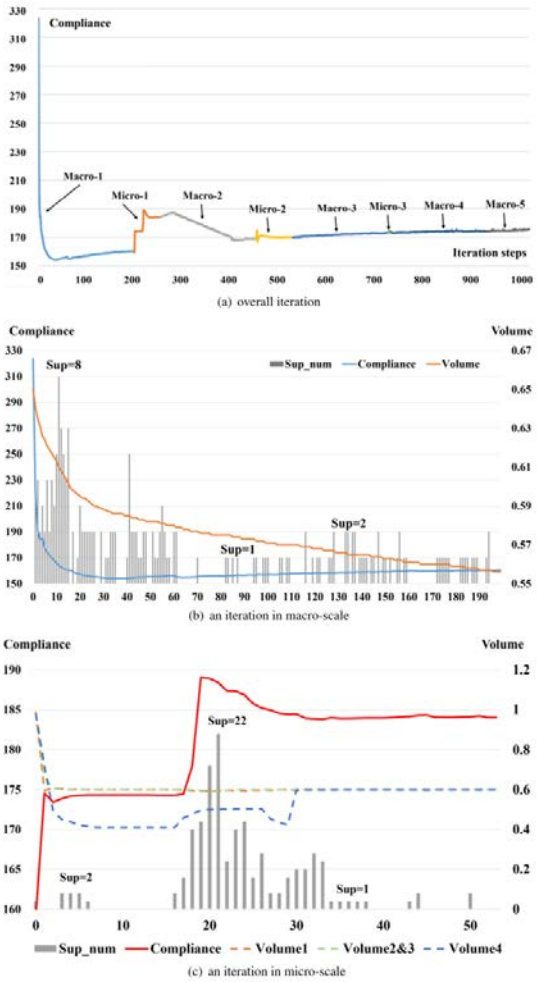

Figure 12. The compliance and volume variation during the iterations for the example in Fig.11.

The convergence curve of the overall iteration process is depicted in Fig.12(a). Specifically, during the overall steps, the macrostructure topology optimization is first conducted with a maximal iteration number of 200. The produced structure gives an initial design domain for the microstructure topology optimization to start with. The micro-scale topology optimization usually converges in a few steps, giving an optimal microstructure for the current macro-scale design. The above described steps are iteratively performed until convergence; see also the overall approach in Fig.3. It is also interesting to note that the micro-scale optimization almost converges without further iterations in the last few overall iteration loops.

Further convergence details on the first macro-scale iteration loop and on the first micro-scale loop are also respectively depicted in Figs.12(b),(c). In Fig.12(b), the blue and orange lines respectively represent variations of the compliances and volume fractions. In addition, the heights of the gray bars represent the number of unsupported elements, where an auxiliary background grid shows the height units. As can be observed, the compliance first decreases sharply and then falls into a stationary state. The number of unsupported elements increases at first and then becomes constant, to one or zero, after several steps of iterations.

In Fig.12(c), the red solid line and the dashed line respectively represents variations of the compliance of the overall structure and the volume fraction of the microstructures. Here, the orange dashed line shows the volume fraction of first-type elements, the green one shows those of the second- and third- type elements, and the blue one shows that of the fourth-type elements. In addition, the gray bars represent variation of the total numbers of unsupported elements. We also note that the compliance of the overall structure mainly depends on the structure of first-type elements which occupies more than \$90\%\$ of the overall structure, as can be observed from the example in Fig.5(b).

5.2 2D bridge at distributed force

Fig.13 shows a 2D bridge problem in a rectangle domain of size 150×50 with a distributed vertical loading at the upper edge, and each macro-element consists of 30×30 square micro-elements. The total number of micro-elements becomes 4500×1500 in this case. The target volume fraction is 40% at the macro-scale and 60% at the micro scale. The printing direction is determined from top to bottom.

The final produced results are shown in Fig.13, where the macrostructure, the produced print-ready structure in micro-scale, and the associated microstructures for the four different types of macro-elements are respectively shown in (a),(b) and (c-f). A close-up of the produced print-ready structure at the microscale is also plotted in Fig.13(b). The proposed approach produces the expected self-supporting structure for the design problem at distributed forces.

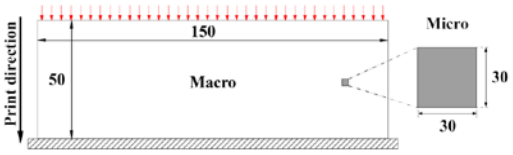

Figure 13. The design domain of a two-scale bridge problem.

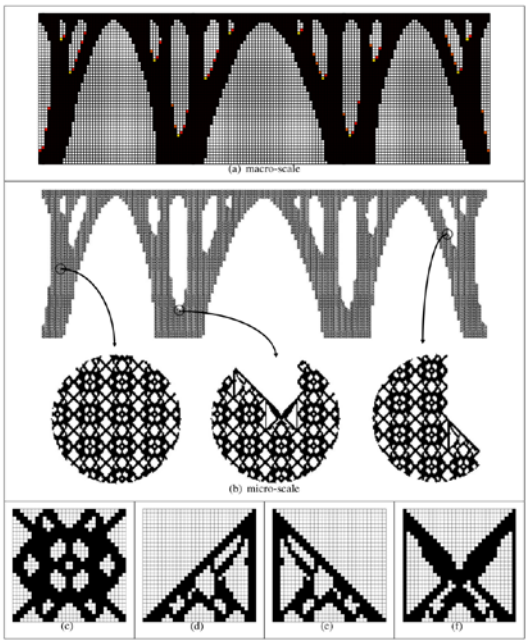

Figure 14. The produced self-supporting biscale structure for the bridge example in Fig.13, where the four micro-structures for the four types of macro-elements in Fig.5 are plotted in the bottom.

5.3 3D wheel

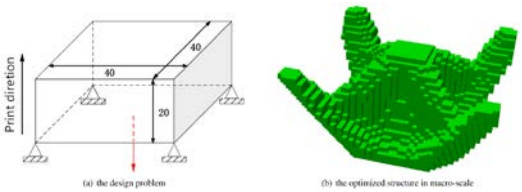

Figure 15. The problem of a two-scale 3D wheel is in (a). The optimized macro-structure is shown in (b), each of which consists of one of the nine types of microstructures listed in Fig.16.

The proposed biscale topology optimization approach under self-supporting constraint was also implemented and tested for 3D examples. Fig.15(a) shows a 3D wheel

problem of size $20 \times 20 \times 10$, exerted by a vertical loading at the center of the bottom. The design domain in the micro-scale consists $10 \times 10 \times 10$ unit cubes. The total number of volume elements is 4,000,000. The target volume fraction is 25% in macro-scale and 40% in micro-scale. The printing direction is determined from bottom to up. The final produced macro-structure is shown in Fig.15(b), which consists of 9 types of microstructures as listed in Fig.16. The overall structure achieved an optimal compliance satisfying the self-supporting constraint ready to be printed without additional usage of support structures.

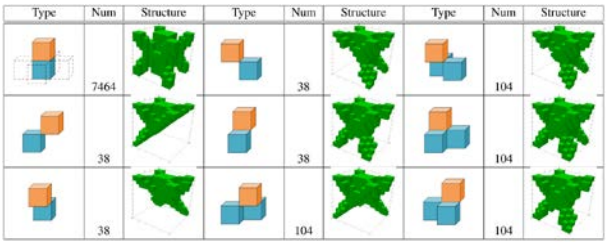

Figure 16. The computed 9 types of optimal micro-structures, each of which is embedded in the macro-elements as a result for the 3D wheel example in Fig.15.

6 Numerical performances

As can be seen from the numerical results, an overall self-supporting structure of large scale is achieved using the proposed approach. This is the first approach that includes self-supporting constraint into biscale topology optimization both for 2D and 3D cases. Simply including self-supporting constraints fir the macro- structure and separately for each micro-structure cannot ensure it. It has to take into account of the gap between the two scales by classifying the macro-elements into four (2D) or sixteen (3D) types, and respectively optimize them. A carefully designed convolution operator much improves the algorithmic efficiency, and a novel and proper definition of the self-supporting constraints simplifies the optimization procedure.

The proposed approach can be improved in the following aspects. Firstly, due to the homogenization approach applied, the structural simulation is not as accurate as direct simulation in micro-scale. As a consequence, the overall biscale topology optimization approach may not converge to a stable solution. In addition, the intrinsic average property of the homogenization approach does not full take into account of the geometry of the microstructure, and thus may even produce disconnected micro-structures. More accurate biscale numerical homogenization approach, such as FE^2 [38], may help to resolve the issue.

Secondly, the self-supporting constraint is included as a local constraint in the present work. The constraint thus may vary when the intermediate generated structure varies during the iteration steps, which may raise convergence issues. Introducing other approach to define the self-supporting constraint and devising an appropriate optimization approach is worthy of future research efforts.

Thirdly, the micro-structures, expect for some special one, are assumed to be of the same geometry. The assumption is made so that the study is focused on building an overall self-supporting structure, and to bridging gaps between the macro- and micro- scales. It however on the other hand also deteriorates performance of the final optimized structure. Taking into account of micro-structures of different geometries on the other hand will raise various other challenges, such as computational efficiency, homogenization accuracy, and is to be studied in our future work.

References

[1] M. Langelaar, An additive manufacturing filter for topology optimization of print-ready designs, Structural and Multidisciplinary Optimization (2016) 1–13.

[2] M. Langelaar, Topology optimization of 3D self-supporting structures for additive manufacturing, Additive Manufacturing 12 (2016) 60–70.

[3] T. Daniel, The development of design rules for selective laser melting, University of Wales.

[4] J. Majhi, R. Janardan, J. Schwerdt, M. Smid, P. Gupta, Minimizing support structures and trapped area in two-dimensional layered manufacturing, Computational Geometry 12 (3-4) (1999) 241–267.

[5] J. Vanek, J. Galicia, B. Benes, Clever support: Efficient support structure generation for digital fabrication, Computer Graphics Forum 33 (5) (2014) 117–125.

[6] C. Wang, Y. Chen, Thickening freeform surfaces for solid fabrication, Rapid Prototyping Journal 19 (6) (2013) 395–406.

[7] J. Dumas, J. Hergel, S. Lefebvre, Bridging the gap: Automated steady scaffoldings for 3D printing, Acm Transactions on Graphics 33 (4) (2014) 1–10.

[8] J. Wu, C. C. Wang, X. Zhang, R. Westermann, Self-supporting rhombic infill structures for additive manufacturing, Computer-Aided Design 80 (2016) 32–42.

[9] K. Hu, S. Jin, C. C. Wang, Support slimming for single material based additive manufacturing, Computer-Aided Design 65 (2015) 1–10.

[10] D.Brackett, I.Ashcroft, R.Hague, Topology optimization for additive manufacturing, in: Proceedings of the Solid Freeform Fabrication Symposium, Austin, TX, 2011, pp. 348–362.

[11] A. T. Gaynor, J. K. Guest, Topology optimization for additive manufacturing: considering maximum overhang constraint, in: 15th AIAA/ISSMO multidisciplinary analysis and optimization conference, 2014, pp. 16–20.

[12] X. Qian, Undercut and overhang angle control in topology optimization: A density gradient based integral approach, International Journal for Numerical Methods in Engineering 111 (3) (2017) 247–272.

[13] X. Guo, J. Zhou, W. Zhang, Z. Du, C. Liu, Y. Liu, Self-supporting structure design in additive manufacturing through explicit topology optimization, Computer Methods in Applied Mechanics & Engineering 323.

[14] X. Huang, S. W. Zhou, Y. M. Xie, Q. Li, Topology optimization of microstructures of cellular materials and composites for macrostructures, Computational Materials Science 67 (2013) 397–407.

[15] X. Yan, X. Huang, Y. Zha, Y. M. Xie, Concurrent topology optimization of structures and their composite microstructures, Computers & Structures 133 (3) (2014) 103–110.

[16] M. P. Bendsoe, N. Kikuchi, Generating optimal topologies in structural design using a homogenization method, Computer Methods in Applied Mechanics & Engineering 71 (2) (1988) 197–224.

[17] M. P. Bendsoe, Optimal shape design as a material distribution problem, Structural Optimization 1 (4) (1989) 193–202.

[18] Y. M. Xie, G. P. Steven, A simple evolutionary procedure for structural optimization, Computers & Structures 49 (5) (1993) 885–896.

[19] X. Huang, Y. M. Xie, A further review of eso type methods for topology optimization, Structural & Multidisciplinary Optimization 41 (5) (2010) 671–683.

[20] M. Y. Wang, X. Wang, D. Guo, A level set method for structural topology optimization, Advances in Engineering Software 192 (1) (2004) 227–246.

[21] N. P. V. Dijk, K. Maute, M. Langelaar, F. V. Keulen, Level-set methods for structural topology optimization: a review, Structural & Multidisciplinary Optimization 48 (3) (2013) 437–472.

[22] X. Qian, Topology optimization in b-spline space, Computer Methods in Applied Mechanics & Engineering 265 (3) (2013) 15–35.

[23] O. Sigmund, K. Maute, Topology optimization approaches, Structural & Multidisciplinary Optimization 48 (6) (2013) 1031–1055.

[24] E. Andreassen, C. S. Andreasen, How to determine composite material properties using numerical homogenization, Computational Materials Science 83 (2) (2014) 488–495.

[25] X. Liang, P. Breitkopf, Design of materials using topology optimization and energy-based homogenization approach in matlab, Structural & Multidisciplinary Optimization 52 (6) (2015) 1229–1241.

[26] Z. H. Zuo, Y. M. Xie, A simple and compact python code for complex 3D topology optimization, Advances in Engineering Software 85 (2015) 1–11.

[27] S. L. Vatanabe, T. N. Lippi, C. R. D. Lima, G. H. Paulino, E. C. N. Silva, Topology optimization with manufacturing constraints: A unified projection-based approach, Advances in Engineering Software 100 (2016) 97–112.

[28] J. Liu, Y. Ma, A survey of manufacturing oriented topology optimization methods, Advances in Engineering Software 100 (2016) 161–175.

[29] J. P. Groen, O. Sigmund, Homogenization-based topology optimization for high-resolution manufacturable microstructures, International Journal for Numerical Methods in Engineering 113 (8) (2018) 1148–1163.

[30] W. Wang, Y. J. Liu, J. Wu, S. Tian, C. C. L. Wang, L. Liu, X. Liu, Support-free hollowing, IEEE Transactions on Visualization & Computer Graphics PP (99) (2017) 1–1.

[31] Y. Xie, X. Chen, Support-free interior carving for 3D printing, Visual Informatics 1 (1) (2017) 9–15.

[32] D. Zhao, M. Li, Y. Liu, Self-supporting topology optimization for additive manufacturing, arXiv preprint arXiv:1708.07364.

[33] C. Xu, M. Li, J. Huang, S. Gao, Efficient biscale design of semiregular porous structures with desired deformation behavior, Computers & Structures 182 (2017) 284–295.

[34] P. Ming, Numerical methods for multiscale elliptic problems, Journal of Computational Physics 214 (2006) 421–445.

[35] A. Abdulle, A. Nonnenmacher, A short and versatile finite element multiscale code for homogenization problems, Computer Methods in Applied Mechanics and Engineering 198 (37-40) (2009) 2839–2859.

[36] H. Li, Z. Luo, N. Zhang, L. Gao, T. Brown, Integrated design of cellular composites using a level-set topology optimization method, Computer Methods in Applied Mechanics & Engineering 309 (2016) 453–475.

[37] K. Svanberg, The method of moving asymptotes – a new method for structural optimization, International journal for numerical methods in engineering 24 (2) (1987) 359–373.

[38] L. Xia, P. Breitkopf, Concurrent topology optimization design of material and structure within FE2nonlinear multiscale analysis framework, Computer Methods in Applied Mechanics & Engineering 278 (2014) 524–542.